http://www.photogrammetry.ethz.ch/general/persons/devrim_publ.html
The Int.LIDAR Mapping Forum (ILMF'08), Denver, Colorado, US, February 21-22 (only on CD-ROM).

Co-registration of pointclouds by 3D Least Squares matching

Devrim Akca and Armin Gruen

Institute of Geodesy and Photogrammetry, ETH Zurich, CH-8093 Zurich, Switzerland
Tel: +41 44 633 3063, Fax: +41 44 633 1101
(akca, agruen)@geod.baug.ethz.ch
www.photogrammetry.ethz.ch

ABSTRACT

The automatic co-registration of point clouds, representing 3D surfaces, is a relevant problem in 3D modeling. We treat the problem as least squares matching of overlapping surfaces. The surface may have been digitized/sampled point by point using a laser scanner device, a photogrammetric method or other surface measurement techniques. Our proposed method estimates the transformation parameters of one or more 3D search surfaces with respect to a 3D template surface, using the Generalized Gauss-Markoff model, minimizing the sum of squares of the Euclidean distances between the surfaces. This formulation gives the opportunity of matching arbitrarily oriented 3D surfaces. It fully considers 3D geometry. The method derives its mathematical strength from the Least Squares matching concept and offers a high level of flexibility for many kinds of 3D surface correspondence problems. The experiments demonstrate the capabilities of the basic method and the extensions. Examples on the terrain/object modeling, cultural heritage applications, accuracy assessment and change detection are presented.

1. INTRODUCTION

For 3D object modeling data acquisition must be performed from different standpoints. The derived local pointclouds (or surfaces) must be transformed into a common coordinate system. This procedure is usually referred to as co-registration.

In practice special targets, provided by the terrestrial laserscanning vendors (e.g. Zoller+Fröhlich, Leica, Riegl), are mostly used for co-registration of pointclouds. However, such a strategy has several deficiencies with respect to fieldwork time, personnel and equipment costs, and accuracy. In a recent study, Sternberg et al. (2004) reported that registration and geodetic measurement parts comprise 10-20% of the whole project time. In another study, a collapsed 1000-car parking garage was documented in order to assess the damage and structural soundness of the structure. The scanning took 3 days, while the conventional survey of the control points required 2 days (Greaves, 2005). In a project conducted by our research group at Pinchango Alto (Lambers et al., 2007), two persons set the targets to the field and measured with RTK-GPS in 1½ days.

Not only fieldwork time but also accuracy is another important concern. The target based registration methods cannot exploit the full accuracy potential of the data. The geodetic measurement naturally introduces some error, which might exceed the internal error of the scanner instrument. In addition, the targets must be kept stable during the whole scanning campaign. This might be inconvenient with the scanning works stretching over more than one day.

Surface based registration techniques stand as efficient and versatile alternative to the target based techniques. They simply bring the strenuous additional fieldwork of the registration task to the computer in the office while optimizing the project cost and duration and achieving a better accuracy.

In the last decade, the surface based registration techniques have been studied extensively. It is still an active research area. Large number of research activities on the topic demonstrates the relevance of the problem. For an exhaustive literature review we refer to Gruen and Akca (2005) and Akca (2007). Co-registration is crucially needed wherever spatially related data sets can be described as surfaces and have to be transformed to each other. Examples can be given in medicine, computer graphics, animation, cartography, virtual reality, industrial inspection and quality control, spatial data fusion, cultural heritage, photogrammetry, etc.

1.1. Our proposed method

The Least Squares matching (LSM) concept had been developed in parallel by Gruen (1984; 1985a), Ackermann (1984) and Pertl (1984). It has been applied to many different types of measurement and feature extraction problems due to its high level of flexibility and its powerful mathematical model: adaptive Least Squares image matching (Gruen, 1984; Gruen, 1985a), geometrically constrained multiphoto matching (Gruen and Baltsavias, 1988), image edge matching (Gruen and Stallmann, 1991), multiple patch matching with 2D images (Gruen, 1985b), multiple cuboid (voxel) matching with 3D images (Maas, 1994; Maas and Gruen, 1995), globally enforced Least Squares template matching (Gruen and Agouris, 1994), Least Squares B-spline (LSB) Snakes (Gruen and Li, 1996). For a detailed survey, the author refers to Gruen (1996).

If 3D pointclouds derived by any device or method represent an object surface, the problem should be defined as a surface matching problem instead of 3D pointcloud matching. In particular, we treat it as Least Squares matching of overlapping 3D surfaces, which are digitized/sampled point by point using a laser scanner device, the photogrammetric method or other surface measurement techniques. This definition allows us to find a more general solution for the problem as well as to establish a flexible mathematical model in the context of the Least Squares matching.

The mathematical model is aimed to be a generalization of the Least Squares image matching, in particular the method given by Gruen (1984; 1985a). The Least Squares image matching estimates the location of a synthetic or natural template image patch on a search image patch, modifying the search patch by an affine transformation, minimizing the sum of squares of the grey level differences between the image patches. Geometric and radiometric differences are simultaneously modeled via image shaping parameters and radiometric corrections.

One decade after, Maas (1994), Maas and Gruen (1995) introduced a straightforward extension of the 2D technique to 3D voxel space, working with volume data rather than image data. The so-called Least Squares cuboid matching method matches and tracks 3D cuboids in 3D image sequences. It has been shown to be very useful in a 3D LIF (laser-induced fluorescence) research project at ETH Zurich (Switzerland). The goal of this project was the measurement and analysis of chemical mixing (reaction) processes under turbulent flow.

This work attempts to give another straightforward extension of the Least Squares matching concept for the 3D surface matching case. The basic estimation model is derived based on those two inspiring works that are Least Squares image matching and Least Squares cuboid matching. It conceptually stands between these two approaches.

Although the registration of 3D pointclouds is a very active research area in many disciplines, there is still the need for a contribution that responds favorably to the following aspects: matching of data sets with higher order spatial transformation models, matching of full 3D surfaces (as opposed to 2.5D), a rigorous mathematical formulation for high accuracy demands, a flexible model for further algorithmic extensions, mechanisms and statistical tools for internal quality control, and capability of matching of data sets in different quality and resolution.

3D object modeling can be a cumbersome task in many cases. The object might be very large or complex, which needs many standpoints for data acquisition. These multiple surfaces should be co-registered under one reference system efficiently, accurately and simultaneously. Some individual pointclouds might not contains sufficient surface information, e.g. for plane or spherical parts of an object surface. The problem can be overcome, if the intensity or color information of object surface is added to the estimation procedure appropriately. The georeferencing, which is the procedure to transform the spatial data from a local system to a higher order object coordinate system, might crucially be needed. As a consequence, we notice that a fully satisfying general solution has still to be found.

This work aims to achieve these goals by proposing a method based on 3D Least Squares matching. The basic estimation model, execution aspects and algorithmic extensions are briefly explained in the next chapter. Chapter three gives the experimental results.

2. LEAST SQUARES 3D SURFACE MATCHING

2.1. The Basic estimation model

$f(x, y, z)$, being the template surface, is a discrete 3D function, which represents an object surface. $g(x, y, z)$, being the search surface, is its conjugate part, which was digitized from a different viewpoint or at a different time or by a different sensor.

Matching is established in an ideal case:

$$f(x,y,z) = g(x,y,z) \tag{1}$$

Because of the effects of random error, Equation (1) is not consistent. Therefore, a true error vector $e(x, y, z)$ is added, assuming that the template noise is independent of the search noise.

$$f(x,y,z) - e(x,y,z) = g(x,y,z) \tag{2}$$

The problem is estimating the parameters of a 3D transformation, which satisfies the least squares matching of the search surface $g(x, y, z)$ to the template $f(x, y, z)$. This is achieved by minimizing a goal function, which measures the sum of the squares of the Euclidean distances between the surfaces.

In order to perform a least squares estimation, Equation (2) is expanded using the Taylor series, of which only the linear terms are retained:

$$-e(x,y,z) = \frac{\partial g^0(x,y,z)}{\partial x}\mathrm{d}x + \frac{\partial g^0(x,y,z)}{\partial y}\mathrm{d}y + \frac{\partial g^0(x,y,z)}{\partial z}\mathrm{d}z - (f(x,y,z) - g^0(x,y,z)) \quad (3)$$

with notations

$$g_x = \frac{\partial g^0(x,y,z)}{\partial x} \quad , \quad g_y = \frac{\partial g^0(x,y,z)}{\partial y} \quad , \quad g_z = \frac{\partial g^0(x,y,z)}{\partial z} \quad (4)$$

where the terms $\{g_x , g_y , g_z\}$ are the numerical first derivatives of the function $g(x, y, z)$ and the terms $\{\mathrm{d}x , \mathrm{d}y , \mathrm{d}z\}$ are the differentiation of the selected 3D transformation model. A 7-parameter 3D similarity transformation is used for the geometric relationship.

After further expansions, Equation (3) gives in matrix notation

$$-\boldsymbol{e} = \mathbf{A}\boldsymbol{x} - \boldsymbol{l} \quad , \quad \mathbf{P} \quad (5)$$

where $\mathbf{A}$ is the design matrix, $\boldsymbol{x}$ is the parameter vector which here contains three translation, one scale and three rotation parameters, $\mathbf{P} = \mathbf{P}_{ll}$ is the a priori weight matrix, and $\boldsymbol{l} = f(x, y, z) - g^0(x, y, z)$ is the discrepancy vector that consists of the Euclidean distances between the template and correspondent search surface elements.

The numerical derivative terms $\{g_x , g_y , g_z\}$ are defined as local surface normals $\boldsymbol{n}$. Their calculation depends on the analytical representation of the search surface elements. Two first degree C^0 continuous surface representations are implemented: triangle mesh form, which gives planar surface elements, and optionally grid mesh form, which gives bi-linear surface elements. The derivative terms are given as *x*-*y*-*z* components of the local normal vectors: $[g_x\ g_y\ g_z]^{\mathrm{T}} = \boldsymbol{n} = [n_x\ n_y\ n_z]^{\mathrm{T}}$.

The parameters are introduced into the system as observables with the associated weight coefficient matrix $\mathbf{P}_b$.

$$-\boldsymbol{e}_b = \mathbf{I}\boldsymbol{x} - \boldsymbol{l}_b \quad , \quad \mathbf{P}_b \quad (6)$$

where $\mathbf{I}$ is the identity matrix and $\boldsymbol{l}_b$ is the (fictitious) observation vector. The joint system Equations (5) and (6) are solved by applying the least squares criteria. The reader is referred to Gruen and Akca (2005) and Akca (2007) for the details of the derivation and solution of Equations (5) and (6).

2.2. Execution aspects

The standard deviations of the estimated transformation parameters and the correlations between them may give useful information concerning the stability of the system and quality of the data content (Gruen, 1985a):

$$\hat{\sigma}_p = \hat{\sigma}_0\sqrt{q_{pp}} \quad , \quad q_{pp} \in \mathbf{Q}_{xx} = (\mathbf{A}^{\mathrm{T}}\mathbf{P}\mathbf{A} + \mathbf{P}_b)^{-1} \quad (7)$$

where $\mathbf{Q}_{xx}$ is the cofactor matrix for the estimated parameters.

The estimated standard deviations of the transformation parameters are optimistic, mainly due to the stochastic properties of the search surfaces that have not been considered as such in the estimation model, as is typically done in Least Squares matching (Gruen, 1985a). The omissions are expected to be minor and do not disturb the solution vector significantly. However, the a posteriori covariance matrix will be affected by the neglected uncertainty of the function values $g(x, y, z)$. This deteriorates the realistic precision estimates. More details on this issue can be found in Gruen (1985a), Maas (2000), Gruen and Akca (2005) and Kraus et al. (2006).

Detection of false correspondences with respect to the outliers and occlusions is a crucial part of every surface matching method. We use the following strategies in order to localize and eliminate the outliers and the occluded parts.

A median type of filtering is applied prior to the matching. For each point, the distances between the central point and its *k*-neighborhood points are calculated. In our implementation, *k* is selected as 8. If most of those *k*-distance values are much greater than the average point density, the central point is likely to be an erroneous point on a poorly reflecting surface (e.g. window or glass) or a range artifact due to surface discontinuity (e.g. points on the object silhouette). The central point is discarded according to the number of distances, which are greater than a given distance threshold.

In the course of iterations a simple weighting scheme adapted from Robust Estimation Methods is used:

$$(\mathbf{P})_{ii} = \begin{cases} 1 & \text{if} \quad |(\boldsymbol{v})_i| < K\hat{\sigma}_0 \\ 0 & \text{else} \end{cases} \tag{8}$$

In our experiments K is selected as >10, since it is aimed to suppress only the large outliers. It can be changed according to a desired confidence level. Because of the high redundancy of a typical data set, a certain amount of occlusions and/or smaller outliers do not have significant effect on the estimated parameters. As a comprehensive strategy, Baarda's (1968) data-snooping method can be favorably used to localize the occluded or gross erroneous measurements.

Finally, the correspondences coinciding to mesh boundaries are excluded from the estimation. The mesh boundaries represent the model borders, additionally the data holes inside the model. The data holes are possibly due to occlusions. Rejecting the correspondences on the mesh boundaries effectively eliminates the occlusions.

The convergence behavior of the proposed method basically depends on the quality of the initial approximations and quality of the data content. For a good data configuration case it usually achieves the solution after 5 or 6 iterations.

Two first degree C^0 continuous surface representations are implemented. In the case of multiresolution data sets, in which point densities are significantly different on the template and search surfaces, higher degree C^1 continuous composite surface representations, e.g. bi-cubic Hermit surface, should give better results, of course increasing the computational expense.

2.3. Algorithmic extensions

Two acceleration strategies are employed in order to optimize the run-time. The first strategy is a rapid method for searching the correspondences. We opt for a space partitioning method given by Chetverikov (1991), called boxing. In the original publication, it was given for 2D point sets. We straightforwardly extend it to the 3D case. We combine our 3D boxing structure with a hierarchical local and adaptive nearest neighborhood search. The second acceleration strategy is the simultaneous matching of sub-surface patches, which are selected in cooperative surface areas. It provides a computationally effective solution, since it matches only relevant multi-subpatches rather than the whole overlapping areas.

When more than two pointclouds with multiple overlaps exist, we adopt a two step solution. First, pairwise LS3D matchings are run on every overlapping pairs and a subset of point correspondences is saved to separate files. In the global registration step, all these files are passed to a block adjustment by independent models procedure (Ackermann et al., 1973), which is a well known orientation procedure in photogrammetry.

We also introduce the combined matching approach. When the object surface lacks sufficient geometric information, i.e. homogeneity or isotropicity of curvatures, the basic algorithm will either fail or find a side minimum. We propose an extension to the basic algorithm in which available attribute information, e.g. intensity, color, temperature, etc., is used to form quasisurfaces in addition to the actual ones. The matching is performed by simultaneous use of surface geometry and attribute information under a combined estimation model.

The further conceptual extensions are given as: Least Squares matching of 3D curves, matching of 3D curves or 3D sparse points (e.g. ground control points) with a 3D surface, and a general framework, which can perform the multiple surface matching, intensity matching and georeferencing tasks simultaneously. Although these extensions have not been implemented and tested yet, they are given here due to their prospective applications, especially in 3D modeling, quality control, and spatial data orientation studies.

The basic algorithm and all other extensions (except the ones given as conceptual) were implemented as a stand-alone MS Windows application with a graphical user interface. The software package was developed with the C++ programming language and the OpenGL graphics application programming interface (API) under C++Builder 5 (Borland Inc.) integrated development environment (IDE).

3. EXPERIMENTAL RESULTS

3.1. Tucume

The first experiment is the matching of two photogrammetrically derived DTMs of an area in Tucume (Peru). The horizontal resolution of the DTMs is 5 meters. The DTMs were manually measured as two independent models from 1:10 000 scaled B/W aerial images in one strip at an overlap of 60% in-flight direction. The mass points, in parallel profiles mode with a sampling distance of 20 meters, and breaklines were measured on an analytical stereoplotter WILD S9, and subsequently interpolated to a regular grid with a mesh size of 5 meters. More details are given in Sauerbier et al. (2004).

Although it is only a 2.5D model, it is a good example for the weak data configuration case since the overlapping area is relatively narrow with little information regarding to the surface geometry (Figure 1a). The numerical results of the basic algorithm of the LS3D matching are given in Table 1.

The large number of iterations and high standard deviations for the estimated parameters t_y , ω and κ obviously reflect the existence of the configuration problem, nevertheless the matching process is successful. Note that the theoretical precision of the *y* element of the translation vector is comparable to the DTM resolution. The residuals between the fixed and transformed surfaces show a random distribution pattern, except some occasional measurement and modeling errors (Figure 1b). In this experiment surface geometry alone is enough to obtain an acceptable solution, even if it contains only little information.

Table 1: Numerical results of "Tucume" experiment.

#	Surface type	No. of points	No. of observation equations ($n_l + n_b + n_c$)	No. of iterations	$\hat{\sigma}_0$ (m)	$\hat{\sigma}_{tx}$ / $\hat{\sigma}_{ty}$ / $\hat{\sigma}_{tz}$ (m)	$\hat{\sigma}_{\omega}$ / $\hat{\sigma}_{\varphi}$ / $\hat{\sigma}_{\kappa}$ (1.0e-02 gon)
I	P	12 660	12 660 + 7 + 0	17	1.38	0.16 / 2.74 / 0.20	1.83 / 0.29 / 2.11
	B			15	1.38	0.16 / 2.85 / 0.20	1.84 / 0.30 / 2.19

P: Plane surface representation in triangle mesh form.
B: Bi-linear surface representation in grid mesh form.
n_l , n_b , n_c : Number of observation equations for actual surfaces, parameters and quasisurfaces, respectively.

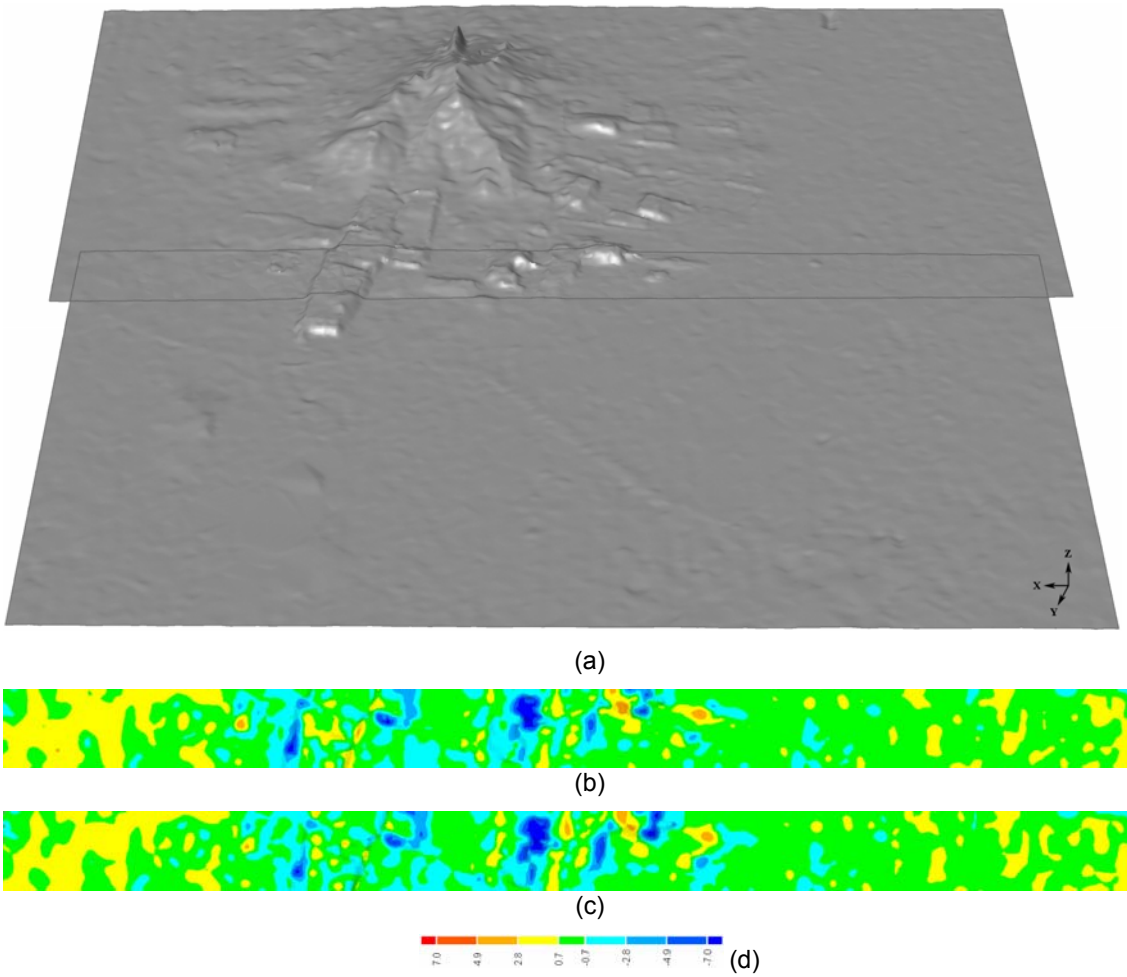

(a)

(b)

(c)

(d)

Figure 11. Experiment "Tucume". (a) The shaded view of the final composite surface after the LS3D surface matching. Note that the overlapping area is delineated by gray borderlines. The colored residuals between the fixed and transformed surfaces after the LS3D matching (b) and the ICP matching (c). The residuals bar unit is meter (d).

A comparison study between the LS3D and ICP was carried out. The registration module of the Geomagic Studio v.6 (Raindrop Geomagic, Inc.) was used as the ICP implementation. Since a statistical

evaluation was not available from Geomagic Studio, we compared the residuals between the fixed and transformed surfaces (Figure 1b and 1c). Both methods show a similar distribution pattern of residuals, but the LS3D gives a slightly better RMS error (1.34 meters) than the ICP (1.42 meters).

3.2. SRTM TerrainScape™ - Filling the holes of SRTM C-Band DEMs

Swissphoto AG (Zurich, Switzerland), in cooperation with Jeppesen (Englewood, Denver, USA), generates a worldwide terrain database that will meet aviation quality requirements for autonomous landing and take-off (Norris, 2005). The base DSM is the Shuttle Radar Topography Mission (SRTM) C-SAR DEM, which covers the Earth's surface between latitudes 60^0N and 57^0S at a resolution of 3 arc second for the full coverage and 1 arc second for the USA and its territories. The Shuttle Radar Topography Mission was jointly performed by the National Aeronautics and Space Administration (NASA), the National Geospatial-Intelligence Agency (NGA), the German Aerospace Center (DLR) and the Italian Space Agency (ASI) in February 2000, to generate a near-global DEM of the Earth using radar interferometry operating in C- and X- bands.

The SRTM C-DEM products have some data holes due to typical problems of radar interferometry (InSAR), e.g. shadows, layover and poor reflectivity properties of the Earth's surface. The project aims to fill these data holes by use of the local DEMs wherever they are available in any resolution and characteristic (Figure 2). Because of the difference in production technique and standards, the local DEMs may have translational shift or/and angular rotation with respect to the SRTM DEMs. In the processing chain, the LS3D software is responsible for correcting these geometric differences by applying the Least Squares 3D surface matching technique. Further information can be found on the project webpage: http://www.photogrammetry.ethz.ch/research/srtm/

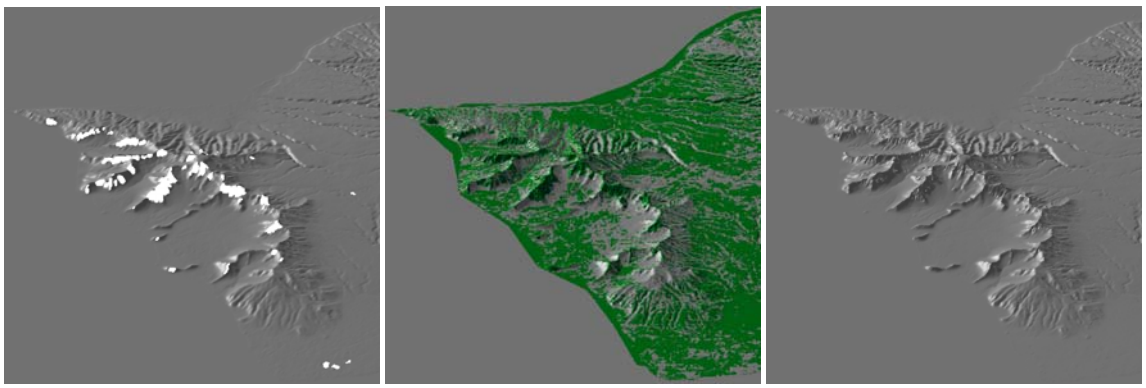

(a) (b) (c)

Figure 2. (a) SRTM C-Band DEM with data holes, (b) registration of a local DEM onto the SRTM C-Band DEM by use of the LS3D matching, (c) filled data holes.

The LS3D software was embedded into the whole package, called SRTM TerrainScape™. The experiments have showed that the LS3D certainly has the capability for the co-registering of multi-resolution and multi-quality data sets. Figure 25 shows the registration of a local DEM with 30 meters resolution to a SRTM C-Band DEM whose resolution is around 90 meters.

3.3. Assessing changes of forest area and shrub encroachment

This is an assessment study of change (1997 – 2002) of forest and other wooded areas in a mire biotope in the Pre-alpine zone of Central Switzerland using airborne remote sensing data. The study is a cooperation between the IGP (ETH Zurich) and the Department of Landscape Inventories of Swiss Federal Research Institute WSL. More details are given in Waser et al. (2007).

The study area is located on a small plateau in the East of the Lake of Zug, a sensitive environmental area in the Pre-alpine zone of Central Switzerland (approx. 47°07' N and 8°32' E). The mire covers an area of 2.61 km2 whereas 1.72 km2 belong to the core area. The altitude varies from 850 m to 1000 m above sea level. The bordering forested area, with an extent of approx. 0.85 km2, is mostly characterized by open mixed forest (40%) and coniferous forest (60%) with some storm losses caused by hurricane Lothar in 1999 and some deforestation in the last years.

Three DSMs generated from two set of CIR-aerial images (year 1997 and 2002) and an airborne laser scanning point cloud (year 2001) were used. There are 4 CIR-aerial images (1 strip) of 1997 and 12 (2 strips) of 2002. Table 2 gives an overview of the image data used in this study.

Table 2. Characteristics of the CIR-aerial images.

Imaging parameters	**CIR-aerial images 1997**	**CIR-aerial images 2002**
Camera	RC 30	RC 30
Acquisition date	04/08/1997	08/07/2002
Image scale	1:10,000	1:5,500
Focal length	21 cm	30 cm
Spectral resolution	Green: 500-600, Red: 600-700, NIR: 750-1000 nm	
Scan/Ground pixel size	15 µm / 15 cm	15 µm / 8.25 cm
Radiometric resolution	8 bit	8 bit
Overlap	Forward: 75%	Forward: 75%, Sideward: 30%

All images were digitized with a Vexcel UltraScan scanner. The 1997 film images had severe scratches on the emulsion side, causing artifacts in the digitized images and DSM errors in the automated DSM generation. Image orientation was established with 15 ground control points measured by a differential GPS survey and with using bundle adjustment of SocetSet V5.2. The sigma naught of orientation was 0.20 pixel and 0.23 pixel for 1997 and 2002, respectively.

Two DSMs were generated automatically from the above images of the years 1997 and 2002 respectively, using SAT-PP (Figure 3). It uses a coarse-to-fine hierarchical matching method with an effective combination of several image matching algorithms and automatic quality control (Zhang and Gruen, 2004). The DSMs have a grid spacing of 0.5 m.

National LIDAR data of the Swiss Federal Office of Topography (Swisstopo) was acquired in 2001 with leaves off. From the raw data, both a DTM and DSM were generated by Swisstopo. The average density of the DSM data was 1-2 points / m2 and the height accuracy (1 sigma) 0.5 m for open areas and 1.5 m for terrain with vegetation. The DTM had an average point density of 0.8 points / m2 and a height accuracy (1 sigma) of 0.5 m. The DSM and DTM were interpolated to a regular grid with 2.5m grid spacing.

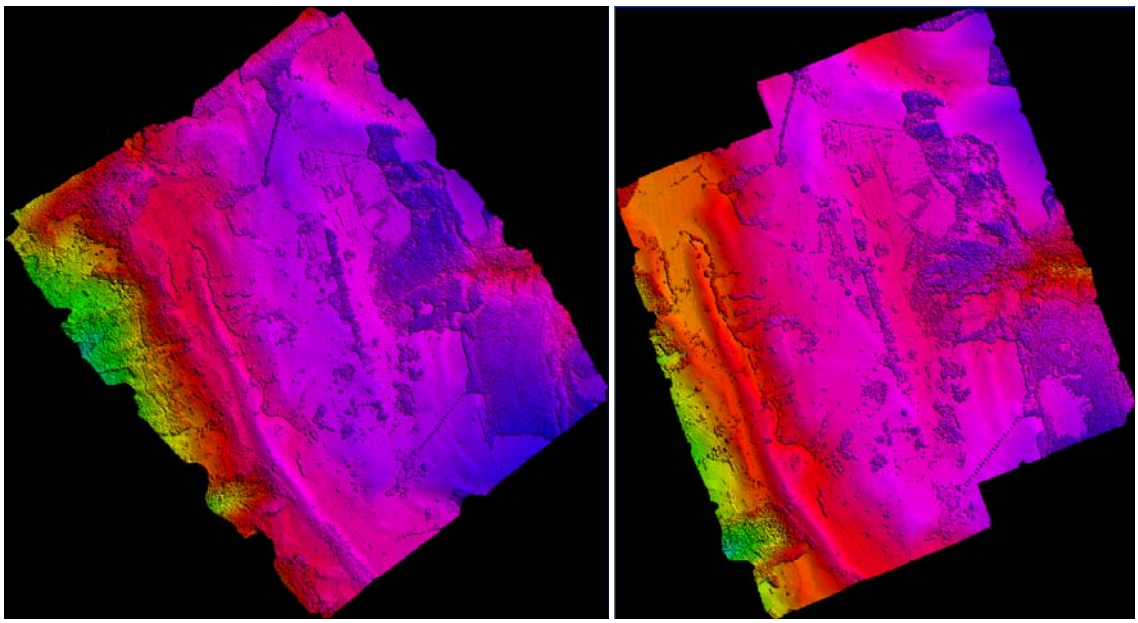

Figure 3. Color coded DSMs from 1997 (left) and 2002 (right). Significant deforestation in 2002 is apparent, especially on the bottom right part of the model.

The matching DSMs of 1997 and 2002, and the LIDAR DSM and DTM were co-registered using the LS3D surface matching method. The co-registration uses a 7-parameter 3D similarity transformation to remove systematic differences (bias) between two datasets, e.g. due to different image orientation. For the estimation of these parameters, we used control surfaces, i.e. DSM parts that did not change in the two datasets, i.e. bare ground, and also removed large differences due to matching errors with a robust filtering. Among the 7 parameters, only the three X, Y, Z shifts were significant in this case. After co-registration, the Euclidian distances between the two datasets are computed as well as the X, Y, Z components, the latter being more important for these investigations. After co-registration, different products could be generated and conclusions drawn. The difference 2002-1997 matching DSM gives the

changes between the two epochs, especially regarding vegetation. After co-registration, the Z-component of the Euclidian distances (sigma a posteriori) was 3.4 m, showing a clear reduction of vegetation from 1997 to 2002.

The difference matching DSMs minus LIDAR DTM gives the normalized DSMs, i.e. the 3D objects in the scene and especially the canopy models. The LIDAR DSM was also subtracted from the 2002 DSM, in spite of the small time difference. This could give a comparison between the two DSMs and also an indication to what extent LIDAR penetrates the tree canopy more compared to matching, a characteristic that was observed in previous studies (see Baltsavias et al., 2006). After co-registration, the Z-component of the Euclidian distances (sigma a posteriori) was 0.8 m, however, there is no indication as to whether the LIDAR or the matching DSM is more accurate. Results are shown in Figures 4 and 5.

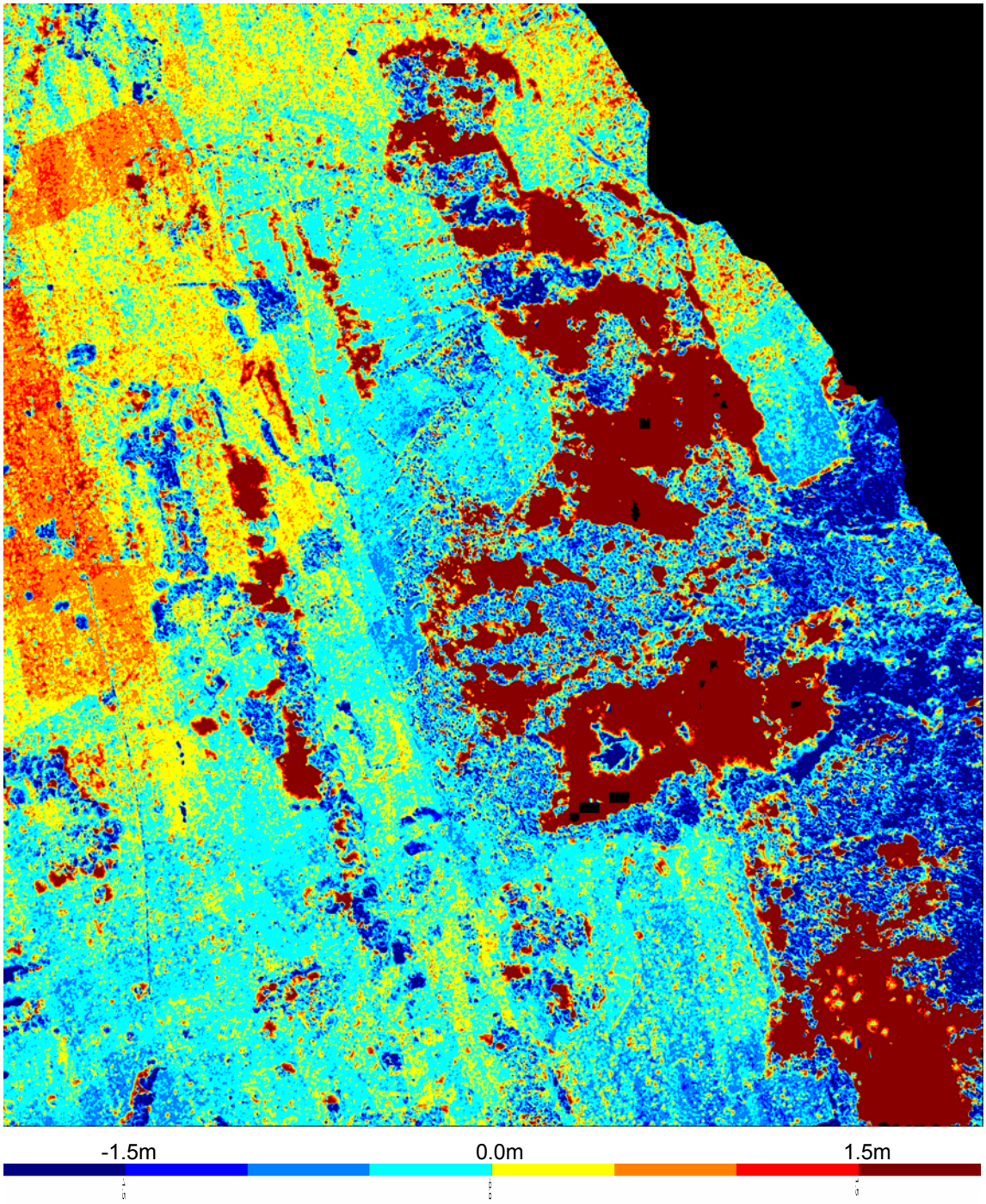

Figure 4. The Z component of the Euclidian distances between 1997 and 2002 matching DSMs shows clearly areas of deforestation and shrub encroachment. The 2002 matching DSM is the reference surface and the 1997 matching DSM is the transformed one. Red areas show the deforestation.

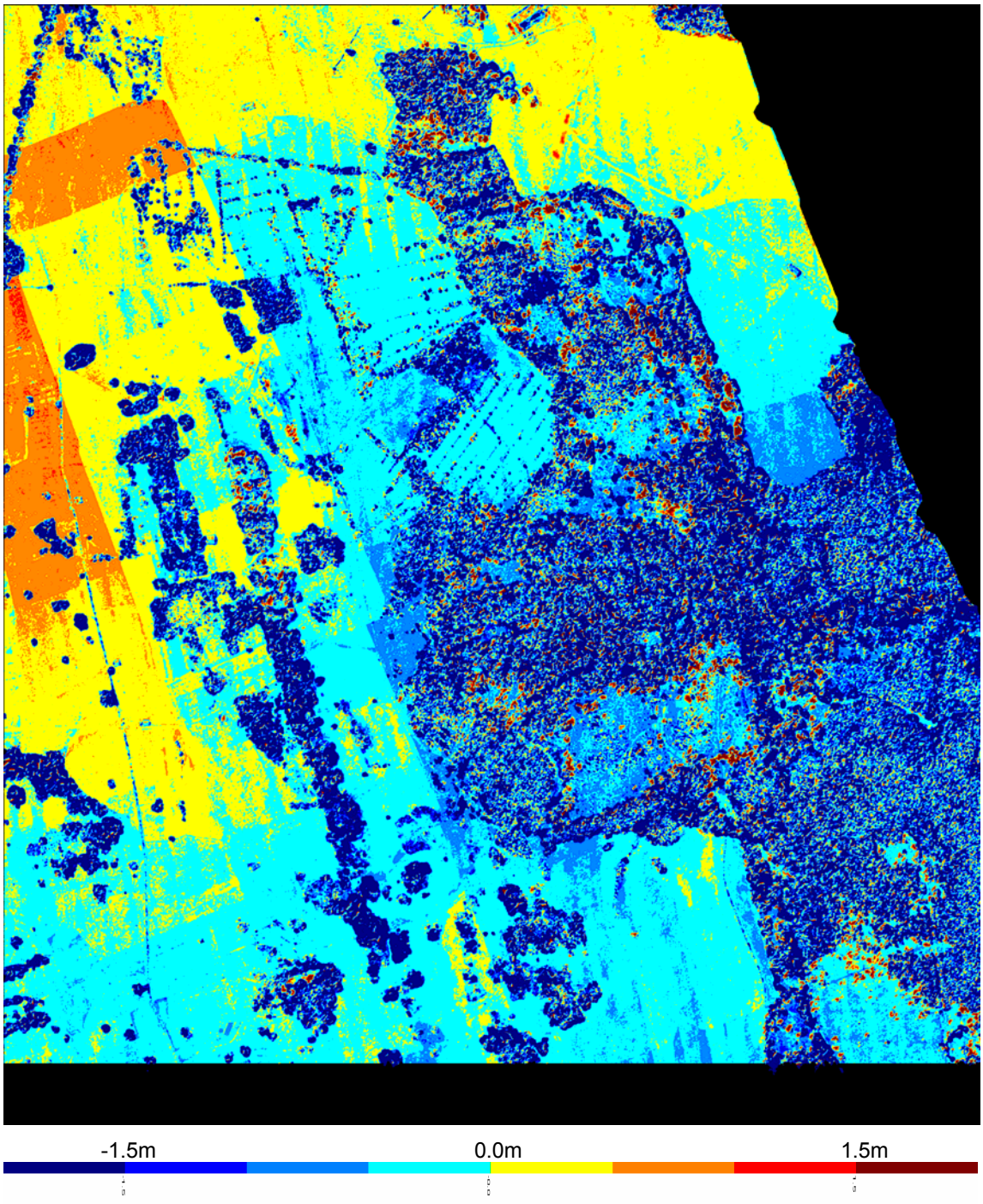

Figure 5. The Euclidian distances between the 2001 LIDAR DSM (search) and the 2002 matching DSM (template) showing that LIDAR measures tree canopies lower than the image matching. At the top and bottom, the effect of the stripes in the matching DSM, possibly due to film scanner (geometric) miscalibration is visible. The orange areas at the top left are due to differences in image orientation between the two flight strips and within each strip causing discontinuities in the 2002 matching DSM. These areas are also visible in Figure 29 but have less sharp boundaries due to the noise of the 1997 matching DSM. The small red spots, mostly inside the forest, show the loss of individual trees during one year time difference.

3.4. Accuracy assessment of the SRTM C-Band DEMs

We compare the SRTM DEM with respect to a reference DEM whose quality and production details are known by us. The reference DEM was generated from optical satellite imagery and processed by use of SAT-PP.

The LS3D is run in three different degree of freedom (DOF) modes, i.e. 6 DOF with rotation and translation parameters, 3 DOF with only translation parameters, and 0 DOF without any transformation. Based on the initial experiments, it was found that the scale factor is not significant. So, the 7 DOF version with the full set of parameters was skipped.

The initial values are given as 0.0 for the rotation and translation parameters. The estimated parameters show the existence of possible rotation and positional shift differences between the coordinate systems. The sigma naught value is a quality measure for the final agreement of the surfaces.

Coordinate values of the template and the search surfaces are not centered before the matching. This leads high (algebraic) correlations between the rotation angles and translation elements, as seen significant differences between the translation elements of the 3 DOF and 6 DOF versions in Tables 4 and 5.

3.4.1. Reference DEM - Hobart

The test site (147^0.280E, 42^0.860S) is located in the south part of the island of Tasmania (Australia), close to Hobart city (Figure 31a). It is covered with dense vegetation. The elevation ranges from the mean sea level to 1280 meters. Technical details of the reference DEM are given in Table 3.

Table 3. Technical details of the reference DEM of Hobart.

Test site	Area size Lon x Lat (degree)	Sensor	DEM Resolution (meters)	H-datum V-datum	No. cols x rows	H-accuracy V-accuracy (meters)
AUS	0.15 x 0.13	IKONOS	5	WGS84 WGS84	2511 x 3032	1.0 1.0 – 3.0

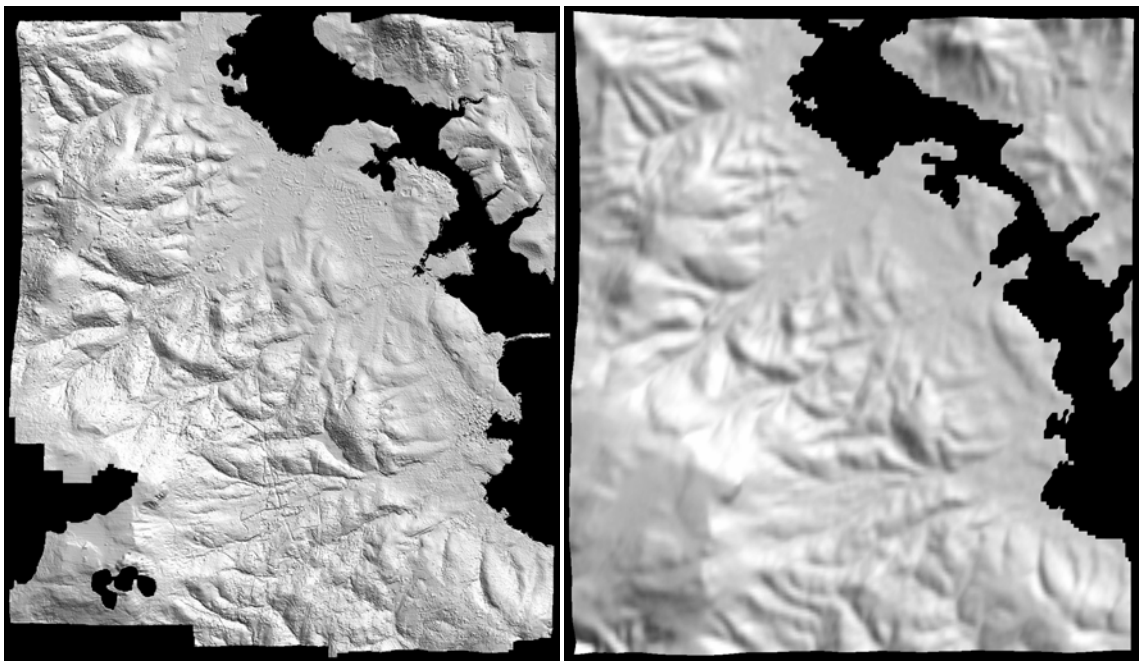

(a) (b)

Figure 6. The reference IKONOS DEM (a) and its corresponding SRTM C-Band DEM (b).

3.4.2. SRTM C-Band DEM – Hobart

The C-Band DEM (Figure 31b) was downloaded from the FTP server of the Land Process Distribution Active Archive Center (LP DAAC). The C-Band DEMs are organized into individual tiles, each of which is a data file with a *.HGT suffix at the file name. Each tile covers an area of 1^0 x 1^0 in longitude and latitude. The horizontal coordinates are given in Geographical Coordinate System (GCS) defined on the WGS84 (World Geodetic System 1984) ellipsoid, while elevations are in meters referenced to the WGS84 EGM96 (Earth Gravitational Model 1986) geoid, which approximates the mean sea level (MSL).

Firstly, the HGT file was converted to the ESRI ASCII grid (*.ASC) format maintaining the unit and reference system of the point coordinate values. This is basically a step to convert the data from binary to ASCII. In a subsequent step, the elevation values were transformed to the ellipsoidal heights so that they

are compatible with the vertical datum of the reference DEM. A 15-minute worldwide geoid height file provided by the National Geospatial-Intelligence Agency (NGA, http://earth-info.nga.mil/GandG/wgs84/gravitymod/) was used in the computation. The geoid undulations were calculated using bi-linear interpolation.

Finally, the ASC files were converted to XYZ point list files (*.XYZ) while transforming the points from the geographical coordinates to the UTM coordinates. This procedure does not perform any resampling. The original resolution is maintained by employing such a conversion strategy. The final XYZ files are in TIN form rather than at a regular grid. The average point spacing is 68 meters along the east direction and 92 meters along the north direction.

The data conversion pipeline is given in Figure 7. All steps of the data conversion were performed using self-developed software.

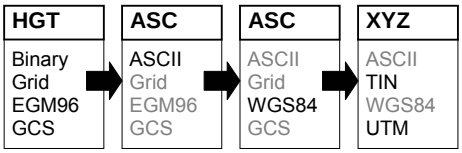

Figure 7. The data conversion pipeline for the C-Band DEM.

3.4.3. Quantitative results of the Hobart test site

The SRTM C-Band DEM (search surface) of the Hobart area was co-registered to the reference DEM (template surface). The results are given in Table 4.

Table 4. Results of the analysis of the C-Band DEM at the test site Hobart.

DOF	No. of valid points	No. of used points Excluded %	Sigma (m) Sigma x/y/z (m)	Mean (m) Min / Max (m)	Tx / Ty/ Tz (m) ω / φ / κ (grad)
0	6,178,111	5,964,655 3.5 %	6.8 1.5 / 1.5 / 6.5	-1.1 -92.0 / 44.4	Na Na
3	6,178,111	5,958,371 3.6 %	6.2 1.3 / 1.3 / 6.0	-0.0 -61.8 / 43.8	-4.58 / -9.66 / 1.59 Na
6	6,178,111	5,958,310 3.6 %	6.2 1.3 / 1.3 / 5.9	-0.0 -61.8 / 44.6	-1.10 / -11.71 / 12.20 -0.008 / 0.012 / 0.005

A small portion of the points (as outliers of the C-Band DEM) was excluded by the robust weighting scheme (Equation 8). The surface co-registrations with 3 DOF and 6 DOF have not improved the sigma a posteriori values significantly. This shows that there is no coordinate system difference between the reference DEM and the C-Band DEM. They are already in agreement. The surface co-registration cleared the -1.08m bias, which is most probably due to penetration property of C-SAR wavelength into vegetation. In Figure 33a, 33b and 33c, blue color shows the areas where C-Band DEM is below the reference IKONOS DEM.

In spite of excluding the 3.6% of large outliers, there are still very large deviations at some spots in the range of -61.8 to +43.8 meters.

3.4.4. Cross-comparison of the SRTM C- and X-Band DEMs – Neuschwanstein

A SRTM X-Band DEM tile, covering an area of 15' x 15' (arc-minute) around Neuschwanstein (Bavaria, Germany) was downloaded from the DLR website: http://www.dlr.de/srtm/produkte/demo_en.htm . The X-Band DEM is in the Digital Elevation Data (DTED) format with *.DT2 suffix at the file name. The same conversion procedure as given in Figure 32 was applied to the X-Band DEM as well, except the vertical datum transformation.

The average point spacing is 18 x 30 meters (along east x north directions) for X-SAR DEM and 62 x 90 meters for C-SAR DEM. Both the X-Band DEM and C-Band DEMs are given in Figure 8.

The X-Band DEM is the template surface, and the search surface C-Band DEM is transformed to the template's reference system.

Without co-registration, the C-Band DEM is clearly above the X-Band DEM with a mean bias value of +2.43 meters. The LS3D co-registration clears this shift value (Figure 9). The co-registration improves the a posteriori sigma value by a factor 2.

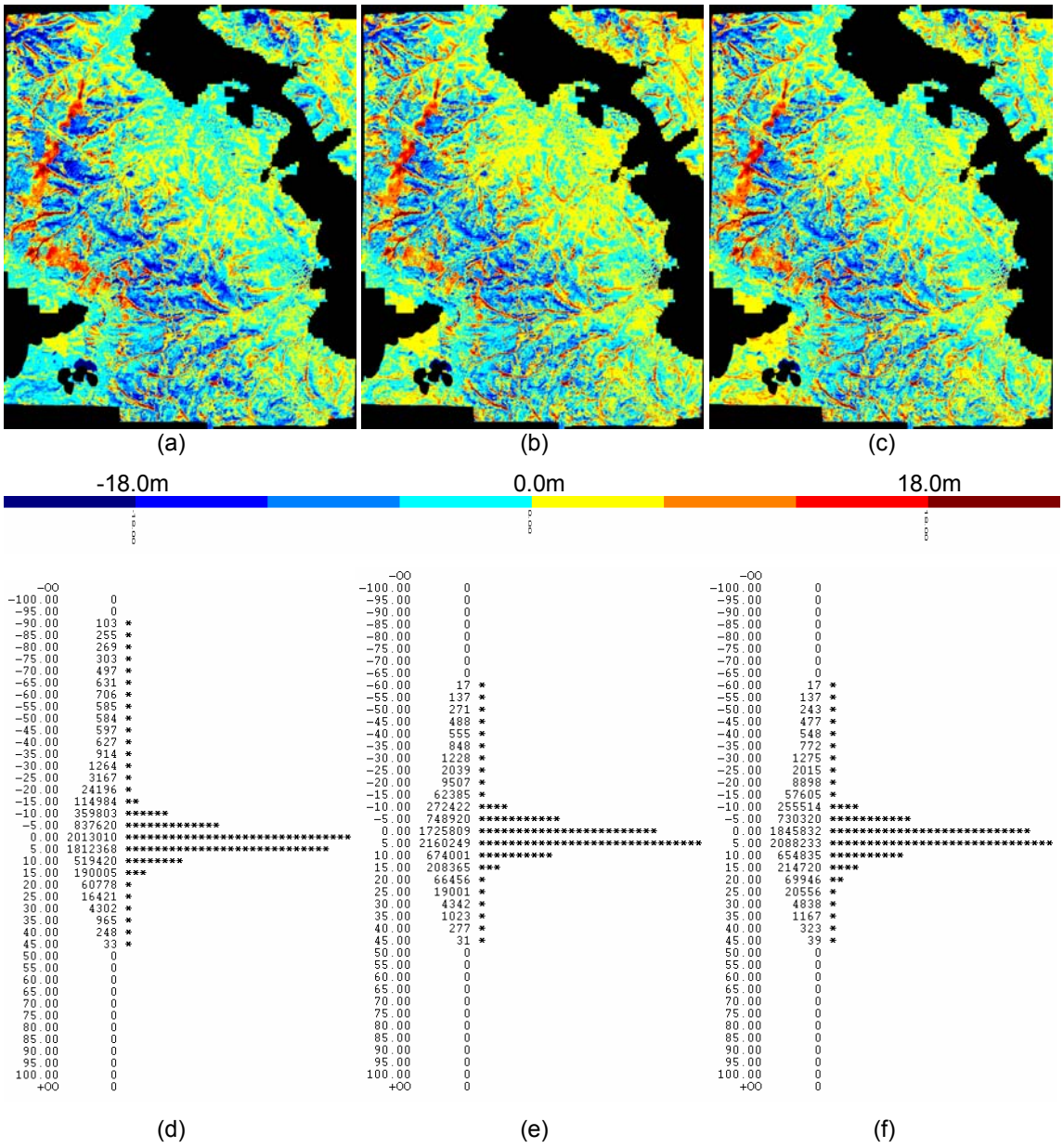

Figure 8. Colored spatial (distance) discrepancies between the reference and C-Band DEMs of the Hobart test site before the LS3D surface matching, i.e. 0 DOF version (a), after the matching of the 3 DOF version (b), and after the matching of the 6 DOF version (c). Frequency distributions of the spatial (distance) discrepancies of the 0 DOF (d), 3 DOF (e) and 6 DOF (f) versions. The residual bar unit is meter.

Table 5. Results of the cross-comparison of the X- and C-Band DEMs at the test site Neuschwanstein.

DOF	No. of valid points	No. of used points Excluded %	Sigma (m) Sigma x/y/z (m)	Mean (m) Min / Max (m)	Tx / Ty/ Tz (m) ω / φ / κ (grad)
0	810,000	804,575 0.7 %	10.8 2.7 / 4.6 / 9.4	2.4 -284.8 / 407.8	Na Na
3	810,000	796,325 1.7 %	6.0 1.3 / 1.8 / 5.5	-0.1 -58.9 / 58.9	0.17 / 5.41 / -3.11 Na
6	810,000	793,802 2.0 %	5.5 1.2 / 1.6 / 5.1	-0.0 -54.1 / 54.5	10.29 / 1.93 / 11.13 -0.013 / -0.004 / 0.009

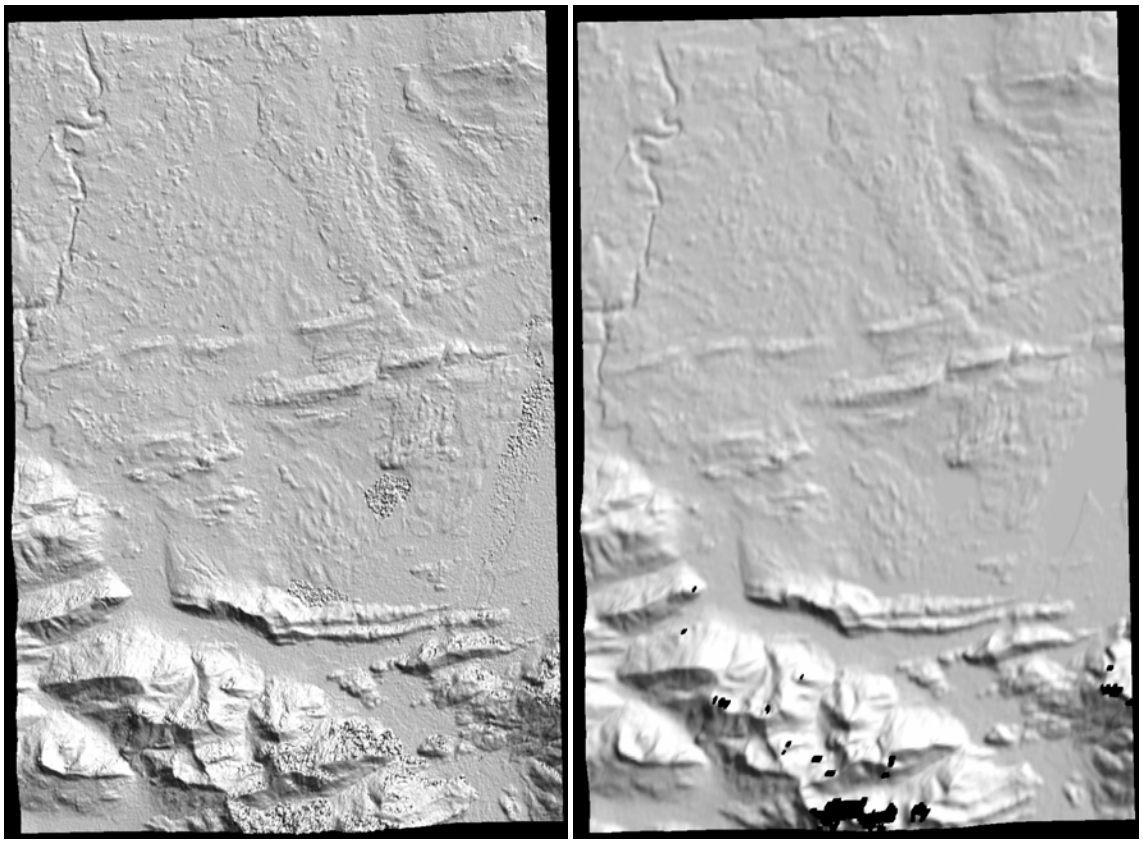

(a) (b)

Figure 9. SRTM X-Band DEM of the Neuschwanstein area (a) and its C-Band DEM counterpart (b).

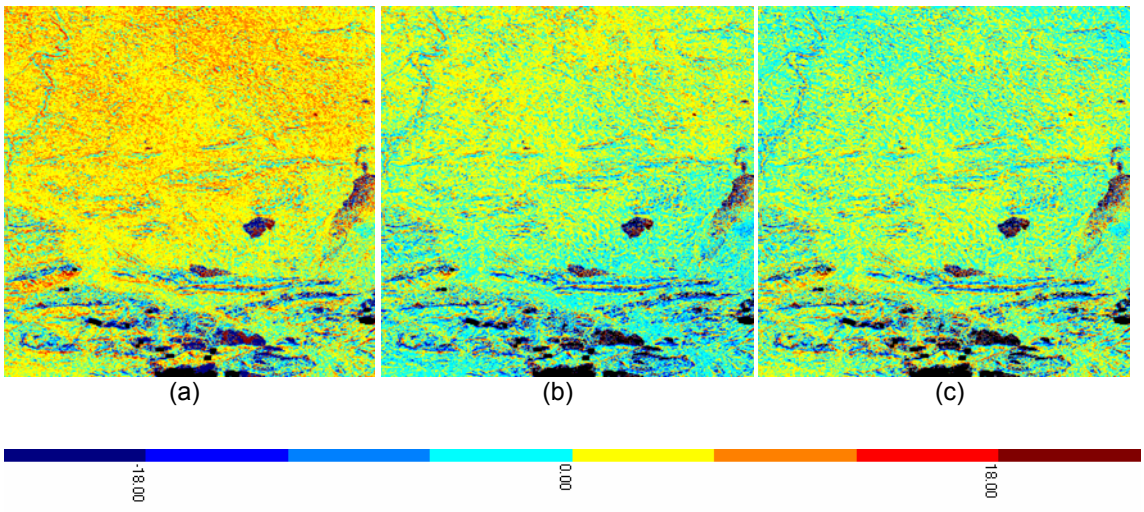

(a) (b) (c)

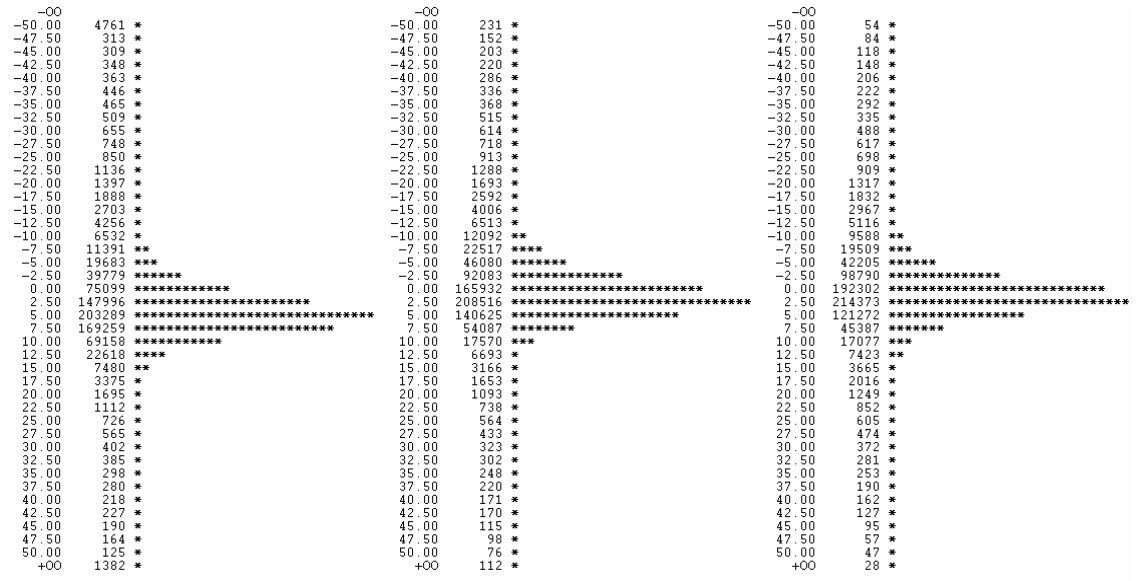

(d) (e) (f)

Figure 10. Cross-comparison between the X- and C-Band DEMs at the test site Neuschwanstein. Colored spatial (distance) discrepancies between the X- and C-Band DEMs for the 0 DOF (a), 3 DOF (b) and 6 DOF (c) versions. Frequency distributions of the spatial (distance) discrepancies of the 0 DOF (d), 3 DOF (e) and 6 DOF (f) versions. The residual bar unit is meter.

3. CONCLUSIONS

Our basic estimation model is a generalization of the Least Squares matching concept for the 3D surface matching problem. It is an algorithmic extension of the early 2D image matching version.

The current implementation uses a 3D similarity transformation model for the geometric relationship. The unknown transformation parameters are treated as observables with proper weights, so that sub-versions of the 7-parameters model can be run, i.e. rigid body, tilt, translation, horizontal shift, depth, etc. If a higher order transformation is demanded, it can easily be introduced.

The LS3D fully considers the 3D information by evaluating the Euclidean distances. The 2.5D surface matching algorithms evaluate the height differences, which is sub-optimal even for terrain surface applications. They cannot consider modeling errors, whereas the proposed LS3D method can do so.

The estimation model is the Generalized Gauss-Markoff model. It is a strict and rigorous formulation, which describes the physical nature of the problem. It provides a flexible mathematical basis, which makes further algorithmic extensions possible.

The Generalized Gauss-Markoff model has a quadratic type of convergence rate. This gives substantially less number of iterations than the ICP variants, whose convergence behavior is monotonic.

The Least Squares concept allows for the monitoring of the quality of the final results by means of precision and reliability criterions. The precision and reliability measures give a quantitative insight into the data content, and help to assess the level of success of the solution. The quality of any individual parameter can be checked via the a posteriori variance-covariance matrix. This feature can be highly important when the data set does not contain sufficient surface information along one or more coordinate directions in order to support the computation of all transformation parameters. The parameters with low precision values help to diagnose and to understand the configuration and content of the data.

3. REFERENCES

Ackermann, F., Ebner, H., and Klein, H., 1973. Block triangulation with independent models. Photogrammetric Engineering and Remote Sensing 39 (9), 967-981.

Ackermann, F., 1984. Digital image correlation: performance and potential application in photogrammetry. Photogrammetric Record 11 (64), 429-439.

Akca, D., 2007. Least Squares 3D surface matching. Ph.D. thesis, Institute of Geodesy and Photogrammetry, ETH Zurich, Switzerland, Mitteilungen Nr.92, 78 pages.
http://www.photogrammetry.ethz.ch/general/persons/devrim_publ.html

Baarda, W., 1968. A testing procedure for use in geodetic networks. Netherlands Geodetic Commission, Delft, Vol. 2, No. 5, 97 p.

Baltsavias, E., Gruen, A., Küchler, M., Thee, P., Waser, L.T., and Zhang, L., 2006. Tree height measurements and tree growth estimation in a mire environment using digital surface models. In Proceedings of Workshop on 3D Remote Sensing in Forestry, 14 – 15 February, Vienna, Austria, 9 p. Available at ftp://igpho.ethz.ch/ub/manos/papers/vienna06_manos.pdf (accessed 23 October 2006).

Chetverikov, D., 1991. Fast neighborhood search in planar point sets. Pattern Recognition Letters 12 (7), 409-412.

Greaves, T., 2005. Laser scanning shaves weeks from failure analysis of parking garage collapse. Spar ViewTM 3 (14), http://www.sparllc.com/archiveviewer.php?vol=03&num=14&file=vol03no14-01 (accessed August 2005).

Gruen, A., 1984. Adaptive least squares correlation – concept and first results. Intermediate Research Project Report to Heleva Associates, Inc., Ohio State University, Columbus, Ohio, March, pp. 1-13.

Gruen, A., 1985a. Adaptive least squares correlation: a powerful image matching technique. South African Journal of Photogrammetry, Remote Sensing and Cartography 14 (3), 175-187.

Gruen, A., 1985b. Adaptive kleinste Quadrate Korrelation und geometrische Zusatzinformationen. Vermessung, Photogrammetrie, Kulturtechnik, 9/85, 309-312.

Gruen, A., and Baltsavias, E.P., 1988. Geometrically Constrained Multiphoto Matching. Photogrammetric Engineering and Remote Sensing 54 (5), 633-641.

Gruen, A., and Stallmann, D., 1991. High accuracy edge matching with an extension of the MPGC matching algorithm. International Conference on Industrial Vision Metrology, Winnipeg, July 11-12, SPIE vol. 1526, pp. 42-55.

Gruen, A., and Agouris, P., 1994. Linear feature extraction by least squares template matching constrained by internal shape forces. International Archives of Photogrammetry and Remote Sensing 30 (3/1), 316-323.

Gruen, A., and Li, H., 1996. Linear feature extraction with LSB-Snakes from multiple images. International Archives of Photogrammetry and Remote Sensing 31 (3B), 266-272.

Gruen, A., 1996. Least squares matching: a fundamental measurement algorithm. In: K. Atkinson (ed.), Close Range Photogrammetry and Machine Vision, Whittles, pp. 217-255.

Gruen, A., and Akca, D., 2005. Least squares 3D surface and curve matching. ISPRS Journal of Photogrammetry and Remote Sensing 59 (3), 151-174.

Kraus, K., Ressl, C., and Roncat, A., 2006. Least squares matching for airborne laser scanner data. 5th International Symposium Turkish-German Joint Geodetic Days, Berlin, March 29-31, (only on CD-ROM).

Lambers, K., Eisenbeiss, H., Sauerbier, M., Kupferschmidt, D., Gaisecker, Th., Sotoodeh, S., Hanusch, Th., 2007. Combining photogrammetry and laser scanning for the recording and modelling of the late intermediate period site of Pinchango Alto, Palpa, Peru, Journal of Archaeological Science 34(10), 1702-1712.

Maas, H.G., 1994. A high-speed solid state camera system for the acquisition of flow tomography sequences for 3D least squares matching. International Archives of Photogrammetry and Remote Sensing 30 (5), 241-249.

Maas, H.G., and Gruen, A., 1995. Digital photogrammetric techniques for high resolution three dimensional flow velocity measurements. Optical Engineering 34 (7), 1970-1976.

Maas, H.G., 2000. Least-Squares Matching with airborne laserscanning data in a TIN structure. International Archives of Photogrammetry and Remote Sensing 33 (3A), 548-555.

Norris, G., 2005. Jeppesen puts synthetic vision system on display. Flight International, 25-31 October, 9-10.

Pertl, A., 1984. Digital image correlation with the analytical plotter Planicomp C-100. International Archives of Photogrammetry and Remote Sensing 25 (3B), 874-882.

Sauerbier, M., Kunz, M., Fluehler, M., and Remondino, F., 2004. Photogrammetric reconstruction of adobe architecture at Tucume, Peru. International Archives of Photogrammetry, Remote Sensing and Spatial Information Sciences 36 (5/W1), (only on CD-Rom).

Sternberg, H., Kersten, Th., Jahn, I., and Kinzel, R., 2004. Terrestrial 3D laser scanning – data acquisition and object modeling for industrial as-built documentation and ar-chitectural applications. International Archives of the Photogrammetry, Remote Sensing and Spatial Information Sciences 35 (B7), 942-947.

Waser, L.T., Küchler, M., Baltsavias, E., Feldmeyer-Christe, E., Eisenbeiss, H., Ginzler, C., Three, P., and Zhang, L., 2007. Assessing changes of forest area and shrub encroachment in a mire ecosystem using digital surface models and CIR-aerial images. Remote Sensing of Environment (accepted for publication).

Zhang, L., and Gruen, A., 2004. Automatic DSM Generation from Linear Array Imagery Data. International Archives of Photogrammetry, Remote Sensing and Spatial Information Sciences 35 (B3), 128-133.